Cell Reports

Report

mTORC2 Assembly Is Regulated by USP9X-Mediated Deubiquitination of RICTOR

Graphical Abstract

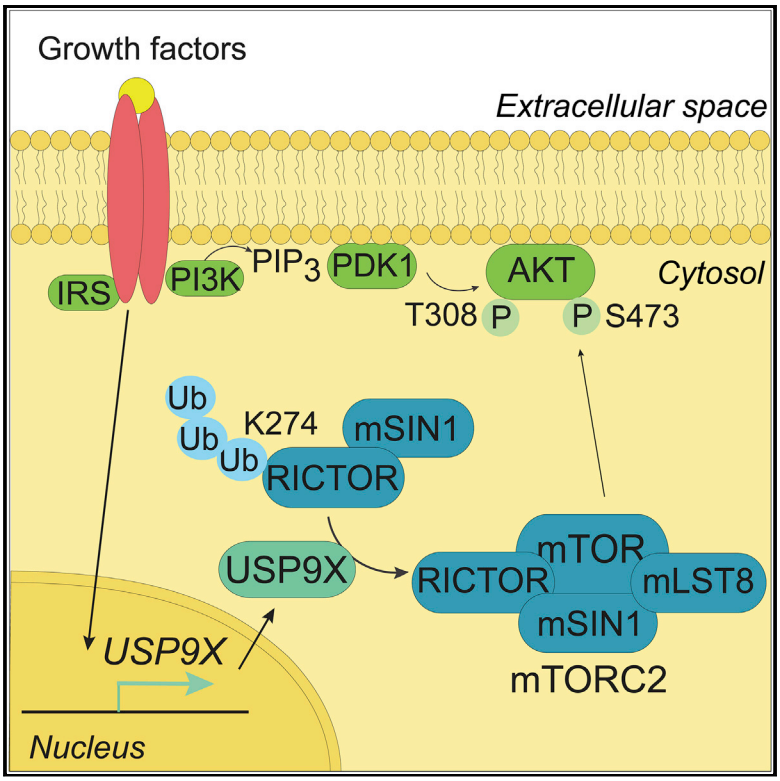

Highlights

- USP9X depletion decreases mTORC2 signaling through RICTOR
- RICTOR ubiquitination regulates the RICTOR-mTOR interaction
- Growth factors regulate *USP9X* expression to regulate hepatic mTORC2 signaling

Authors

Lidia Wrobel, Farah H. Siddiqi, Sandra M. Hill, Sung Min Son, Cansu Karabiyik, Hyunjeong Kim, David C. Rubinsztein

Correspondence

dcr1000@cam.ac.uk

In Brief

The mechanistic target of rapamycin complex 2 (mTORC2) controls cell metabolism and survival. Factors regulating mTORC2 assembly and activity are not well understood. Wrobel et al. provide experimental evidence that growth factor availability stimulates USP9X expression to promote RICTOR assembly into functional mTORC2, thereby facilitating mTORC2 downstream signaling.

Wrobel et al., 2020, Cell Reports *33*, 108564
December 29, 2020
https://doi.org/10.1016/j.celrep.2020.108564

CellPress

Cell Reports

CellPress
OPEN ACCESS

Report

mTORC2 Assembly Is Regulated by USP9X-Mediated Deubiquitination of RICTOR

Lidia Wrobel,[1,2] Farah H. Siddiqi,[1,2] Sandra M. Hill,[1,2] Sung Min Son,[1,2] Cansu Karabiyik,[1,2] Hyunjeong Kim,[1,2] and David C. Rubinsztein[1,2,3,*]

[1]Department of Medical Genetics, Cambridge Institute for Medical Research, University of Cambridge, Hills Road, Cambridge CB2 0XY, UK
[2]UK Dementia Research Institute, Cambridge, UK
[3]Lead Contact
*Correspondence: dcr1000@cam.ac.uk
https://doi.org/10.1016/j.celrep.2020.108564

SUMMARY

The mechanistic target of rapamycin complex 2 (mTORC2) controls cell metabolism and survival in response to environmental inputs. Dysregulation of mTORC2 signaling has been linked to diverse human diseases, including cancer and metabolic disorders, highlighting the importance of a tightly controlled mTORC2. While mTORC2 assembly is a critical determinant of its activity, the factors regulating this event are not well understood, and it is unclear whether this process is regulated by growth factors. Here, we present data, from human cell lines and mice, describing a mechanism by which growth factors regulate ubiquitin-specific protease 9X (USP9X) deubiquitinase to stimulate mTORC2 assembly and activity. USP9X removes Lys63-linked ubiquitin from RICTOR to promote its interaction with mTOR, thereby facilitating mTORC2 signaling. As mTORC2 is central for cellular homeostasis, understanding the mechanisms regulating mTORC2 activation toward its downstream targets is vital for our understanding of physiological processes and for developing new therapeutic strategies in pathology.

INTRODUCTION

The mechanistic target of rapamycin (mTOR) coordinates cellular metabolism and growth in response to environmental and intracellular stimuli, including nutrients and growth factors (Kim and Guan, 2019; Saxton and Sabatini, 2017). The mTOR kinase is the catalytic component of two distinct protein complexes: mTORC1 and mTORC2. mTORC1 contains mTOR, mLST8 (also known as GβL) with the defining subunit RAPTOR, and mTORC2 contains mTOR, mLST8 along with RICTOR and mSIN1. mTORC1 plays a central role in regulating cell growth through protein synthesis, biosynthesis of nucleotides, and autophagy, whereas mTORC2 primarily controls proliferation and survival. mTORC2 was reported to be not only a positive (Renna et al., 2013; Vlahakis et al., 2014) but also a negative regulator of autophagy (Aspernig et al., 2019; Mammucari et al., 2007), depending on the cell type or the organism analyzed. The best-characterized substrates of mTORC1 are S6K and 4E-BP, which control translation (Sonenberg and Hinnebusch, 2009). mTORC2 directly phosphorylates AKT, serum- and glucocorticoid-induced protein kinase 1 (SGK1), and protein kinase C (PKC), thereby regulating cell proliferation, survival, and metabolism (Facchinetti et al., 2008; García-Martínez and Alessi, 2008; Ikenoue et al., 2008; Sarbassov et al., 2004, 2005). Activation of mTORC2 is mainly mediated by extracellular signals from growth factors, and although still debated, this activation is thought to be mediated by phosphatidylinositol 3-kinase (PI3K) signaling (Ebner et al., 2017; Gan et al., 2011; Liu et al., 2015; Xu et al., 2019). Growth-factor-mediated phosphorylation of different mTORC2 subunits (Oh and Jacinto, 2011), association with ribosomes (Zinzalla et al., 2011), or localization at the plasma membrane (Gan et al., 2011; Liu et al., 2015; Yang et al., 2006) have been reported to specifically influence mTORC2 activity, while not affecting complex assembly. While mTORC2 complex assembly is a critical determinant of its activity, the factors regulating this event are not understood, and it is unclear whether this process is regulated by nutrients and signals that stimulate mTORC2 (Jain et al., 2014; Wang et al., 2017).

RESULTS

USP9X Depletion Decreases mTORC2 Signaling through RICTOR

While screening for novel factors involved in autophagy, our preliminary experiments suggested that transient knockdown of ubiquitin-specific protease 9X (USP9X/FAM) in human cervical cancer (HeLa) cells decreased LC3-II levels in the absence and presence of the lysosomal inhibitor bafilomycin A1 (BafA1), indicating that autophagosome formation is impaired (Figure S1A). USP9X is a highly conserved, substrate-specific deubiquitinating enzyme with multiple targets (Chen et al., 2000; Murtaza et al., 2015). As autophagy is regulated by nutrients and by the activities of the mTOR complexes, we assessed the phosphorylation of mTORC1 and mTORC2 targets. First, we tested the efficiency of USP9X knockdown using four different single oligonucleotides in HeLa, SH-SY5Y, HEK293, and HepG2 cells

(Figures S1B–S1E). Small interfering RNA (siRNA)-mediated knockdown of USP9X in HeLa (Figure 1A) and SH-SY5Y neuroblastoma cells (Figure S1F) decreased the phosphorylation of mTORC2 targets: Ser473 and Thr450 in AKT as well as the levels and phosphorylation of PKCα in both cell lines. In agreement, phosphorylation of AKT at Ser473 in response to serum or insulin treatment was significantly impaired when USP9X was depleted in HeLa cells (Figures 1B and S1G) and murine embryonic fibroblasts (MEFs; Figure S1H), with no effect on 4E-BP1 and S6K phosphorylation at mTORC1 sites. Interestingly, phosphorylation of AKT at Thr308 was slightly increased in HeLa but not in MEF cells in response to USP9X knockdown, suggesting a compensatory response to sustain fully activated AKT, essential for rapid cell proliferation. USP9X knockdown reduced mTORC2 substrate phosphorylation, indicating USP9X as a possible specific modulator of mTORC2 activity. Thus, we have focused this study on the action of USP9X in mTORC2 regulation and have not pursued the autophagy angle here.

To further investigate the role of USP9X on mTORC2 activity, we measured the protein levels of mTORC2 components. USP9X knockdown decreased the levels of RICTOR in HeLa and HepG2 liver cells (Figures 1C and S1I) without affecting the levels of mTOR, mLST8, mSIN1, or mTORC1-specific component RAPTOR. USP9X depletion also decreased the association of RICTOR with mTOR (Figure 1D). RICTOR knockdown did not affect USP9X levels, indicating that USP9X acts upstream of RICTOR (Figure S1J). Note that siRNA-mediated RICTOR depletion in HeLa cells decreased AKT-Ser473 phosphorylation to a similar extent as USP9X knockdown (compare Figures 1A and S1J). Endogenous USP9X and RICTOR interacted in HeLa cells (Figures 1E and S1K). The reduction in RICTOR levels after USP9X knockdown in HeLa cells was rescued by a proteasome inhibitor (Figure 1F), suggesting that USP9X protects RICTOR from proteasomal degradation. Indeed, ubiquitination of endogenous RICTOR was increased when USP9X was depleted under proteasome inhibition (Figure 1G), suggesting that loss of USP9X deubiquitinase activity may be responsible for these phenotypes. To test whether USP9X catalytic activity was required to maintain RICTOR levels, we silenced endogenous USP9X gene expression and then expressed either wild-type USP9X or a catalytically dead USP9X (C1566A; USP9X-CD). While RICTOR levels could be restored by the expression of wild-type USP9X, no rescue was seen upon expression of USP9X-CD (Figure 1H), suggesting that USP9X catalytic activity is necessary to maintain RICTOR levels. RICTOR levels were also reduced by a previously described G9 inhibitor, which targets USP9X/USP24/USP5 activities (Figure S1L) (Peterson et al., 2015). USP9X has been shown to preferentially cleave Lys11- and Lys63-linked polyubiquitin chains from its client proteins (Paudel et al., 2019). Indeed, we observed not only an increase in RICTOR Lys63-linked ubiquitination in USP9X knockdown cells but also an increase in degradational Lys48-linked ubiquitination (Figures 1I and 1J) that further supports our observations that RICTOR degradation is accelerated in USP9X-inhibited conditions. To investigate whether the decreased mTORC2 signaling following USP9X depletion was a direct consequence of reduced RICTOR levels, we treated HeLa cells with control or siRNA against USP9X and then restored RICTOR levels through transient transfection with a RICTOR expression construct. We observed a partial rescue of the decreased phosphorylation of mTORC2 targets, such as Ser473 and Thr450 in AKT, Thr32 in FOX03a, or PKCα phosphorylation and levels, suggesting that the observed decrease in mTORC2 signaling in USP9X knockdown cells is specifically triggered by the loss of RICTOR (Figure 1K). Thus, in HeLa cells, USP9X regulates ubiquitination of RICTOR and its stability and influences mTORC2 activity.

USP9X Regulates Lys63-Linked Ubiquitination of RICTOR Lys274

In HEK293 and SH-SY5Y cells, USP9X knockdown reduced AKT-Ser473 phosphorylation, but the levels of RICTOR and other mTOR complex subunits were not changed (Figures 2A, S1F, and S2A). Furthermore, total ubiquitination and Lys63-linked ubiquitination, but not Lys48-linked ubiquitination, of RICTOR was significantly increased upon USP9X knockdown in HEK293 cells (Figures 2B–2D, S2B, and S2C). These results suggest that USP9X-mediated RICTOR ubiquitination has a non-proteolytic function with respect to mTORC2 activity. Analysis of the human ubiquitin-modified proteome indicated three potential sites of ubiquitination within the RICTOR protein (Kim et al., 2011). Mass spectrometry analysis of RICTOR isolated from USP9X-depleted cells compared with control cells revealed Lys274 as a potential USP9X-targeted site, as its ubiquitination was significantly enriched in cells depleted for USP9X (Figure S2D). To validate our finding, we generated a RICTOR expression construct where Lys274 was replaced with Arg (K274R). HEK293 cells depleted for USP9X were then transfected with wild-type or K274R mutant myc-tagged RICTOR. The expression levels of both proteins were similar (Figure 2E, input), but the K274R mutation almost abolished the increased RICTOR ubiquitination upon USP9X knockdown (Figure 2E). Similar results were observed when RICTOR wild-type and mutant were immunoprecipitated using a Lys63-only-ubiquitin construct (able to form only Lys63-linkages), demonstrating that RICTOR Lys274 is a primary site for USP9X-dependent Lys63-linked deubiquitination (Figure 2F). Using an *in vitro* deubiquitination assay, we demonstrated that active USP9X (incubated in 37°C) can hydrolyze Lys63-linked ubiquitin from purified RICTOR wild-type, but not the K274R mutant (Figure 2G). This reaction was blocked by the USP9X inhibitor G9. The decrease in RICTOR wild-type ubiquitination in a sample where no external USP9X was added may be due to residual amounts of USP9X in the elution fraction in purified RICTOR (Figure S2E). Interestingly, mutation of Lys274 stabilized RICTOR levels in HeLa cells with diminished USP9X (Figure 2H). Together, these data show that RICTOR is a direct target of USP9X and that USP9X targets Lys63-linked ubiquitin on RICTOR Lys274.

RICTOR Ubiquitination Regulates the RICTOR-mTOR Interaction

The stability and integrity of the mTORC2 complex are dependent on the presence of the core subunits RICTOR and mSIN1 (Frias et al., 2006; Guertin et al., 2006; Jacinto et al., 2006;

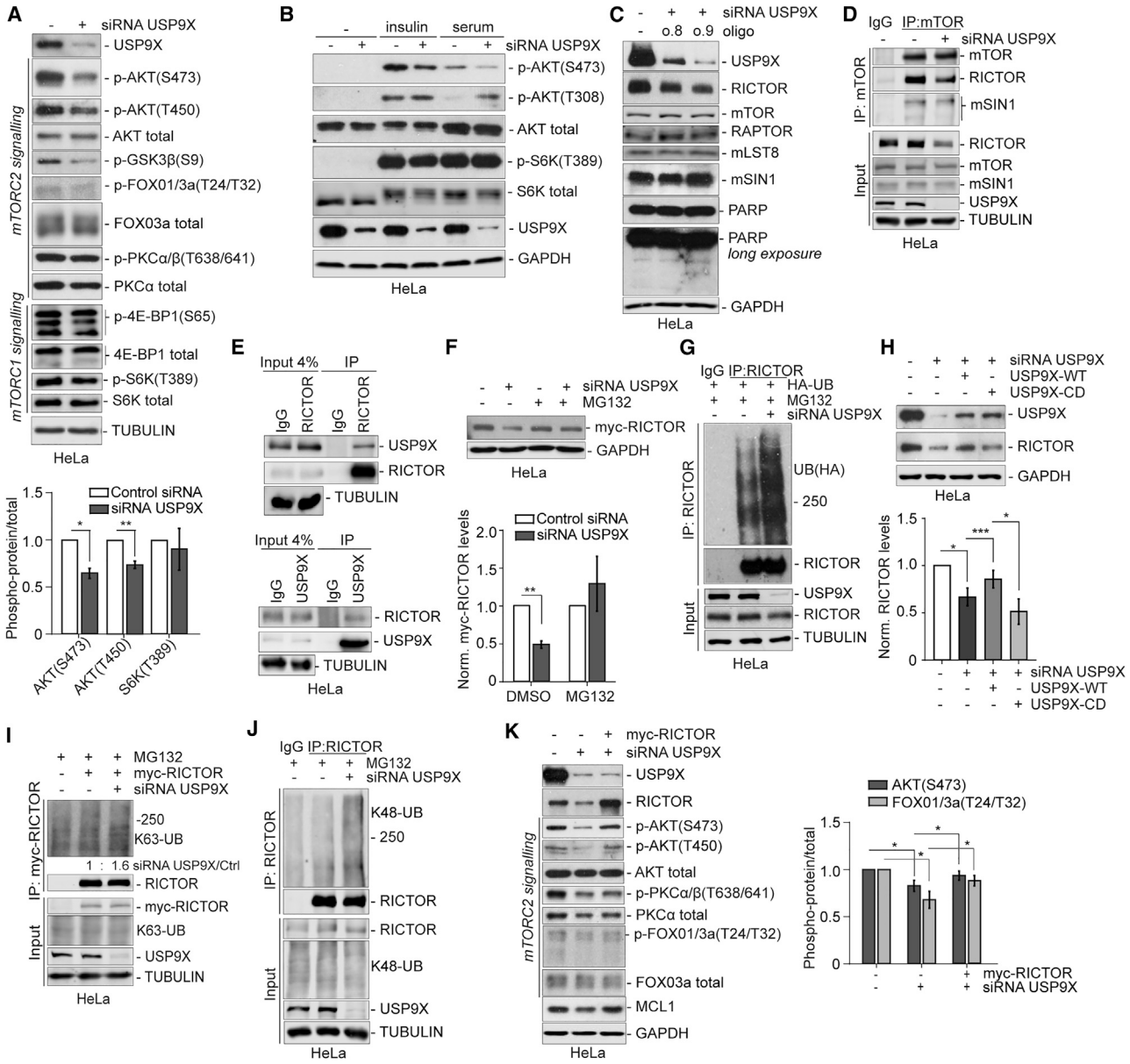

Figure 1. USP9X Promotes mTORC2-Mediated Signaling by Regulating RICTOR

(A–D) Control and USP9X knockdown HeLa cells were lysed (A; n = 3–4, C) or serum starved (B) for 16 h and restimulated for 30 min with insulin or 1 h with full medium before lysis (B) or endogenous mTOR was immunoprecipitated (D).

(E) Endogenous RICTOR or USP9X were immunoprecipitated from HeLa cells.

(F and G) Control and USP9X knockdown HeLa cells were transfected with myc-RICTOR (F) or with HA-ubiquitin (UB) (G) and after 24 h incubated with 5 μM MG132 for 4 h prior to lysis (F; n = 3), or endogenous RICTOR was immunoprecipitated. Ubiquitination signal was detected using anti-hemagglutinin (HA) (G).

(H) HeLa cells expressing doxycycline (Dox)-inducible USP9X-wild type (WT) or -CD mutant (C1566A) were transfected with control or *USP9X* siRNA (oligo 7) for 48 h prior to addition of Dox for 24 h (n = 4).

(I–K) Control and USP9X knockdown HeLa cells were transfected with myc-RICTOR for 24 h (I and K) and lysed (K; n = 4–5) or incubated with 5 μM MG132 for 4 h, and myc-RICTOR (I) or endogenous RICTOR (J) was immunoprecipitated. Ubiquitination signal was detected using anti-Lys63- (I) or anti-Lys48-linkage ubiquitination (J).

For (A)–(K), protein phosphorylation and levels were determined by immunoblotting with the indicated antibodies. Mean ± SEM. Two-tailed paired Student's t test, *p < 0.05, **p < 0.01, and ***p < 0.001. IP, immunoprecipitation.

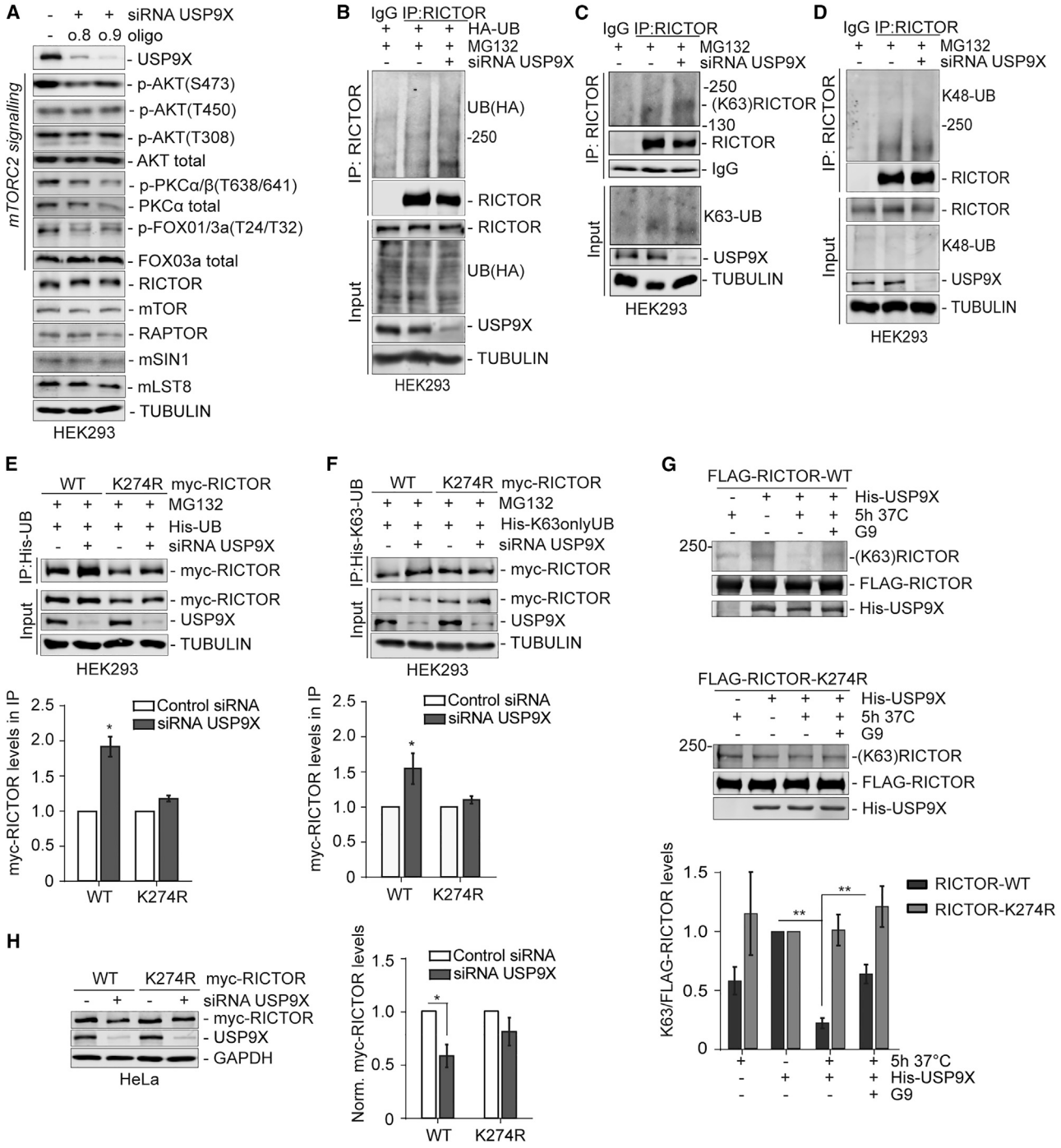

Figure 2. RICTOR Lys274 Is Deubiquitinated by USP9X

(A–D) Control and USP9X knockdown HEK293 cells were lysed (A) or transfected with HA-UB for 24 h (B) and treated with 5 μM MG132 for 5 h (B–D) prior to endogenous RICTOR immunoprecipitation. Ubiquitination signal was detected using anti-HA (B), anti-Lys63-linkage ubiquitination (C), or anti-Lys48-linkage ubiquitination (D).

(E and F) Control and USP9X knockdown HEK293 cells were transfected with myc-RICTOR-WT or K274R together with His-UB (E) or His-Lys63onlyUB (F) and then treated with 5 μM MG132 for 5 h (n = 3 in E, n = 5 in F; one-tailed paired Student's t test).

(G) *In vitro* deubiquitination assay. FLAG-RICTOR and His-USP9X were incubated on ice or at 37°C for 5 h in the presence of 1 μM G9 when indicated (n = 3).

(H) Control and USP9X knockdown HeLa cells were transfected with myc-RICTOR-WT or K274R (n = 3).

For (A)–(F). Protein phosphorylation and levels were determined by immunoblotting with the indicated antibodies. Mean ± SEM. Two-tailed paired Student's t test, if not stated otherwise, *p < 0.05 and **p < 0.01.

Yang et al., 2006). Our earlier experiments suggest that USP9X can affect mTORC2 activity without changing the levels of its subunits (Figures 2A, S1F, and S2A). To assess whether RICTOR ubiquitination could affect mTORC2 activity by altering complex assembly, we compared the interactions of immunoprecipitated mTORC2 components in USP9X knockdown and in control cells (Figures 3A and S2F). Knockdown of USP9X decreased the interaction of mTOR with RICTOR and mSIN1 and simultaneously increased the interaction between mTOR and RAPTOR. Interestingly, the decreased binding between mTOR and mSIN1 in USP9X knockdown cells was more pronounced for the mSIN1.2 isoform (Figures 3A and S2F). Using a proximity ligation assay (PLA), which yields a signal when two proteins are within 40 nm from each other, we confirmed that the interaction between mTOR and RICTOR is largely decreased in USP9X knockdown cells (Figure 3B, PLA controls in Figure S2G). Wild-type and K274R RICTOR interacted similarly with mSIN1 (Figure S2H). Likewise, in HEK293 cells, USP9X knockdown did not alter the interaction between RICTOR and mSIN1, while we did observe a decreased interaction between RICTOR and mTOR, in line with our previous data (Figure 3C). Conversely, overexpression of USP9X in HEK293 cells decreased RICTOR ubiquitination (Figure 3D); increased phosphorylation of AKT at Ser473, without affecting phosphorylation of AKT-Thr308 or S6K (Figure S2I); and increased the interaction between RICTOR and mTOR (Figure 3E). Therefore, we hypothesized that the ubiquitination status of RICTOR Lys274 influences its interaction with mTOR and confirmed that the K274R mutation in RICTOR increased the interaction between RICTOR and mTOR (Figure 3F). To further validate our findings, we used CRISPR-Cas9 to generate a HEK293 monoclonal RICTOR knockout cell line. We confirmed that RICTOR knockout depletes phospho-(p-) AKT-Ser473, but not p-S6K-Thr389 and that RICTOR knockout does not change the levels of USP9X, in line with our previous observations (Figure 3G). Overexpression of RICTOR wild-type and RICTOR-K274R rescued the levels of p-AKT-Ser473 in cells where USP9X was still present and able to deubiquitinate RICTOR efficiently (Figure 3H). However, presence of the K274R mutation prevented the decrease in mTORC2 activity toward AKT-Ser473 in cells where USP9X was knocked down, suggesting that lack of ubiquitination on RICTOR Lys274 is sufficient to sustain mTORC2 activity in USP9X-depleted conditions (Figure 3I). This is consistent with our assertion that RICTOR Lys274 is a primary site for USP9X deubiquitination and that RICTOR-K274R binds mTOR more efficiently compared with wild-type RICTOR, further supporting the idea that USP9X-mediated hydrolysis of ubiquitin from RICTOR promotes mTORC2 assembly. Although mTOR complexes in HeLa, HEK293, SH-SY5Y, and HepG2 cells contain similar amounts of mTOR, the amount of RICTOR bound to mTOR varies between cell lines, and this binding does not correlate with its levels in the input, suggesting that there is always a free pool of RICTOR present in cells (Figure S2J). It is likely that the loss of USP9X activity in HeLa and HepG2 cells leads to more rapid RICTOR degradation as the larger uncomplexed RICTOR pool may be more prone to ubiquitin-proteasomal degradation in these cells, compared with HEK293 and SH-SY5Y cells.

Growth Factors Regulate USP9X Expression to Regulate Hepatic mTORC2 Signaling

We observed that depletion of serum or all nutrients, but not just glucose (Glc) or amino acids alone, decreased USP9X levels in HeLa cells (Figure 4A). One hour of depletion of serum or all nutrients, but not just Glc or amino acids, decreased *USP9X* promoter transcriptional activity (Figures 4B and S3A). Furthermore, inhibition of the type-1 insulin growth factor receptor (IGFR-1) using BMS-536924, but not inhibition of mTOR using mTORC1/2 inhibitor Torin1, decreased *USP9X* promoter activity (Figure S3B), followed by a decrease in USP9X (Figure S3C). As RICTOR's half-life in HeLa cells is ~10 h and the decrease in RICTOR levels follows the decrease in USP9X levels, we observed a significant decrease in RICTOR levels after 10 h of starvation (Figures S3C and S3D). Refeeding with full nutrient medium caused a rapid increase in promoter activity, which was independent of mTOR kinase activity as it was still observed in the presence of Torin1 (Figures 4C and S3E). In agreement, *USP9X* mRNA levels were increased by serum addition (Figure 4D), followed by an increase in the USP9X and RICTOR protein levels through *de novo* synthesis, as this was blunted by cycloheximide (Figure S3F). Serum refeeding decreased RICTOR ubiquitination in serum-starved HeLa and HEK293 cells (Figures S3G–S3H). The increase of USP9X levels was diminished when IGFR-1 was inhibited, but not upon mTOR inhibition, further supporting that *USP9X* expression is regulated by growth factor availability upstream of mTOR (Figure 4E). Interestingly, USP9X knockdown did not prevent the increase in RICTOR levels after 2 h of refeeding, but it strongly blunted phosphorylation of AKT-Ser473, indicating inhibition of mTORC2 (Figure 4F). This further confirms that *USP9X* expression is regulated by external growth factors to promote mTORC2 activity through regulation of RICTOR-mTOR binding.

To confirm the relevance of our findings *in vivo*, we analyzed the levels of USP9X and RICTOR in different mouse tissues and found that they correlate and displayed the highest levels in liver and brain (Figure S4A). The liver is a key organ in insulin-mediated regulation of metabolism, and mTORC2 is crucial for proper liver function as liver-specific *Rictor* knockout mice have impaired glycolysis and lipogenesis, accompanied by systemic metabolic changes (Hagiwara et al., 2012; Yuan et al., 2012). We analyzed the liver from fed and fasted mice and found a significant decrease in Usp9x and Rictor levels after fasting (Figures 4G and S4B) as well as decrease in *Usp9x* mRNA (Figure 4H), consistent with our observations in cells. Disruption of mTORC2 in mice by homozygous *Rictor* deletion causes embryonic lethality (Guertin et al., 2006), and *Usp9x* depletion from mouse embryos halts development at the blastocyst stage (Pantaleon et al., 2001). To study the role of Usp9x *in vivo*, we utilized siRNA injections to transiently knock down *Usp9x* expression in mice. Analysis of blood and plasma parameters showed no difference in Glc and insulin between control and *Usp9x* siRNA-treated mice (Figure S4C). As *Usp9x* siRNA-treated female mice had increased alanine aminotransferase (ALT) in the blood, indicating liver damage (Figure S4C), only male mice were

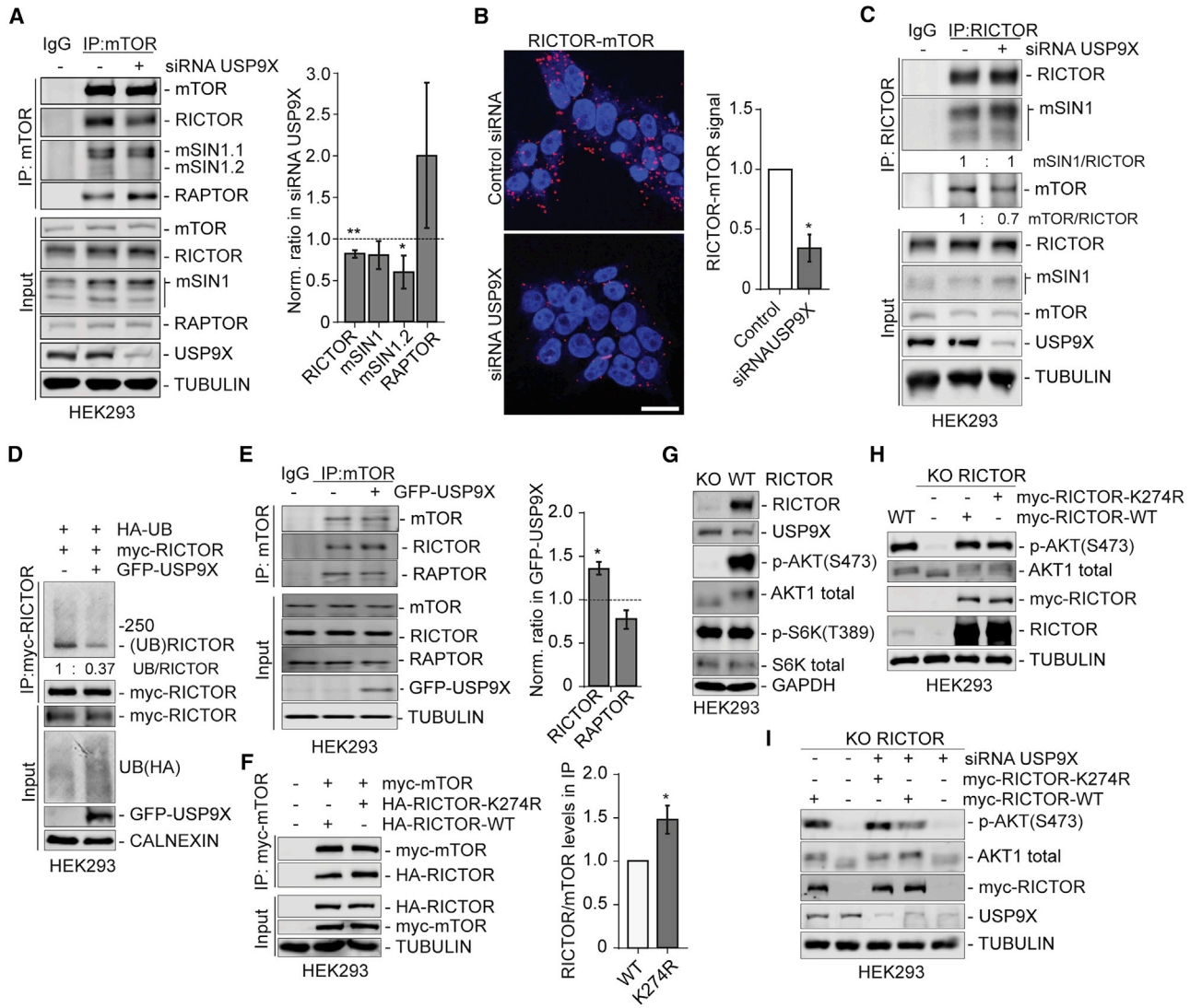

Figure 3. RICTOR Lys274 Deubiquitination by USP9X Promotes RICTOR-mTOR Interaction and mTORC2 Signaling

(A and B) Control and USP9X knockdown HEK293 cells were lysed, and endogenous mTOR was immunoprecipitated (A; n = 4–5) or fixed and analyzed by PLA assay (B; n = 3). PLA negative controls in Figure S2G. Scale bar, 10 μm.

(C) Endogenous RICTOR was immunoprecipitated from control and USP9X knockdown HEK293 cells.

(D and E) HEK293 cells were transfected with GFP-USP9X construct together with myc-RICTOR-WT and HA-UB for 48 h. RICTOR ubiquitination was detected using anti-HA (D), or endogenous mTOR was immunoprecipitated (E; n = 3).

(F) HEK293 cells were transfected with HA-RICTOR-WT or K274R together with myc-mTOR, and myc-mTOR was pulled down (n = 3).

(G) Protein levels analysis in HEK293 WT (non-targeting guide RNA [gRNA] control) and RICTOR knockout (KO) cells.

(H) HEK293 RICTOR KO cells were transfected with myc-RICTOR-WT or K274R for 24 h.

(I) HEK293 RICTOR KO cells were transfected with control or *USP9X* siRNA for 48 h and then transfected with myc-RICTOR-WT or K274R for 24 h.

For (A) and (C)–(I), protein phosphorylation and levels were determined by immunoblotting with the indicated antibodies. Mean ± SEM. Two-tailed paired Student's t test, *p < 0.05 and **p < 0.01.

analyzed further. *Usp9x* siRNA-treated mice had significantly decreased Usp9x protein levels in liver tissue, despite no detectable changes at the level of *Usp9x* mRNA (Figure S4D). As hepatic mTORC2 is required for insulin-activated AKT signaling, we aimed to examine mTOR effectors in the liver of mice refed after fasting. Analysis of blood and plasma parameters of fasted and refed mice showed the expected increase in Glc and insulin levels in both control and *Usp9x* knockdown mice upon refeeding (Figure S4E). Surprisingly, the mRNA of *Usp9x* was again not reduced and actually tended to increase in mice treated with siRNA against *Usp9x* (Figure S4F). This contrasts with the protein levels, which decreased with *Usp9x* siRNA (Figures 4I, 4J, S4D, and S4G). In all of our *Usp9x* siRNA-treated mice, we observed decreased protein levels, but not mRNA. This unexpected finding may be explained by translational repression where the siRNA downregulates the translation of the target mRNA without

CellPress
OPEN ACCESS

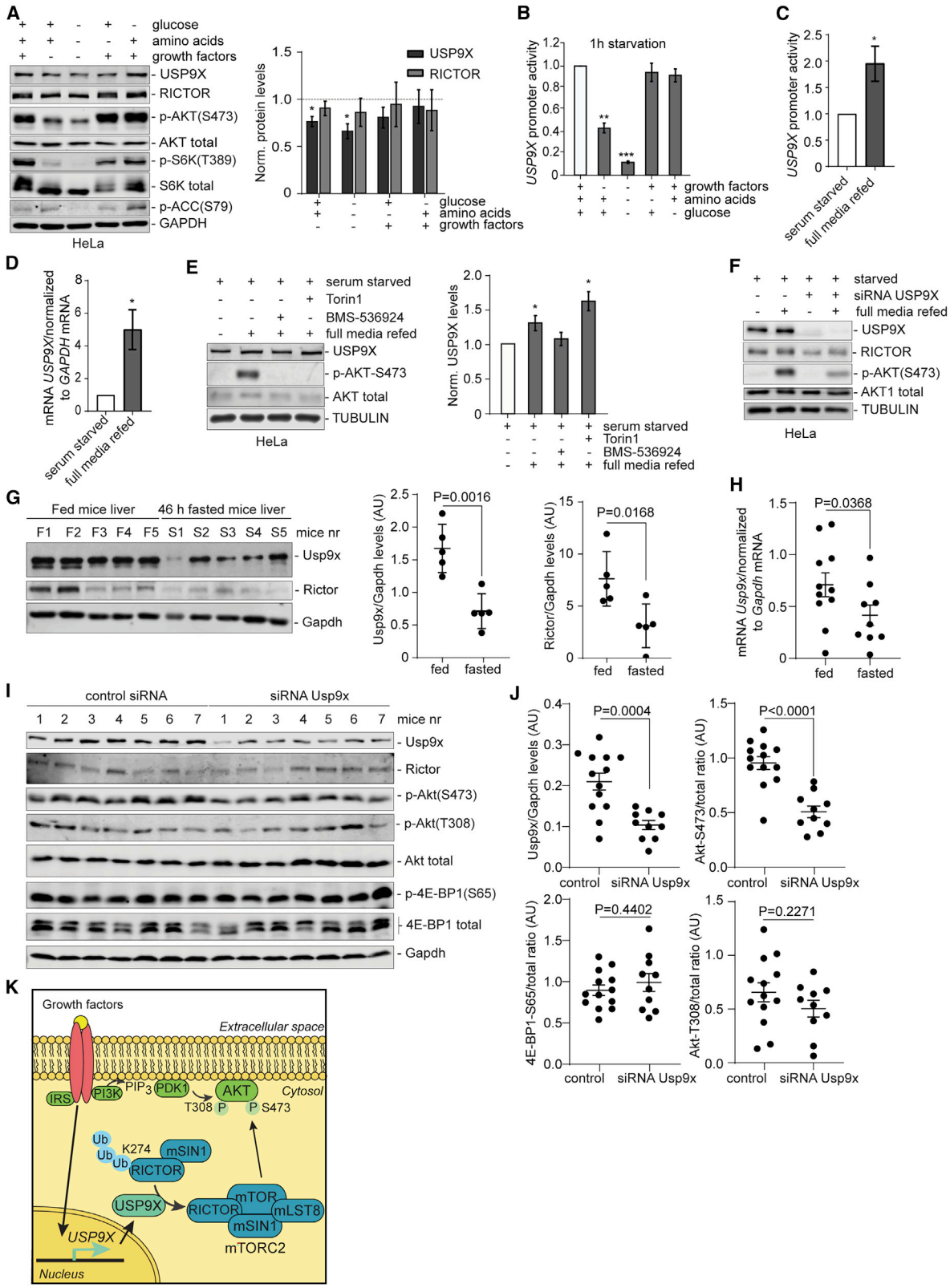

(legend on next page)

inducing detectable mRNA cleavage or reducing mRNA expression levels (Wu and Belasco, 2008; Zeng et al., 2003). *Usp9x* siRNA-treated mice showed significant decreases in Usp9x protein levels, and most importantly refeeding of these mice failed to stimulate phosphorylation of the mTORC2-specific downstream effector Akt-Ser473, whereas phosphorylation of Akt-Thr308 and mTORC1-specific 4E-BP1-S65 was unaffected (Figures 4I, 4J, and S4G), consistent with our observations in cells. Thus, growth factors stimulate *USP9X* expression to promote RICTOR assembly into functional mTORC2 to regulate its downstream targets (Figure 4K).

DISCUSSION

We have identified a mechanism by which mTORC2 assembly and consequent activity are regulated upstream of mTOR by USP9X activity. USP9X knockdowns in HeLa, HEK293, SH-SY5Y, and MEF cells specifically disrupted mTORC2 signaling, represented by diminished phosphorylation of downstream targets, without affecting phosphorylation of mTORC1-specific targets, which we confirmed in mouse livers. Thus, in the cells and mice that we studied, we have no obvious effects on mTORC1 signaling but impaired mTORC2 signaling after USP9X knockdown, in contrast to what was described previously in differentiating skeletal muscle cells (increased mTORC1 and mTORC2) (Agrawal et al., 2012) and in neuronal progenitors (decreased mTORC1) (Bridges et al., 2017). It is possible that these discordant results may reflect processes in differentiating cells in the previous studies.

Our data suggest that mTORC2 signaling is decreased upon USP9X knockdown due to increased RICTOR ubiquitination. The increase in RICTOR ubiquitination prevented RICTOR and mSIN1 from interacting with mTOR, while leaving the interaction between RICTOR and mSIN1 unaffected. This confirms previous reports that RICTOR can bind mSIN1 without prior association with mTOR (Chen et al., 2018; Yang et al., 2006). mSIN1 isoforms were reported to define unique mTORC2s, and both isoforms 1 and 2 ensure mTORC2 plasma membrane localization (Ebner et al., 2017; Frias et al., 2006). Interestingly, we observed that USP9X knockdown leads to a more pronounced decrease in binding of the mSIN1.2 isoform to mTOR, compared with the mSIN1.1 isoform, suggesting that USP9X-mediated RICTOR deubiquitination might favor assembly of a specific pool of mTORC2 containing mSIN1.2.

Structural and experimental reports show that the binding of RICTOR and RAPTOR to mTOR are mutually exclusive (Chen et al., 2018; Sarbassov et al., 2004; Stuttfeld et al., 2018). USP9X knockdown cells were characterized by a decreased association of RICTOR with mTOR but increased RAPTOR and mTOR binding. Conversely, increasing the levels of USP9X decreased RICTOR ubiquitination and subsequently increased the interaction between RICTOR and mTOR and decreased the RAPTOR-mTOR association. Moreover, we showed that presence of ubiquitin on RICTOR Lys274 prevents it from complexing with mTOR, possibly by spatial disruption, as Lys274 is positioned on the domain mediating the RICTOR-mTOR interaction (Chen et al., 2018; Stuttfeld et al., 2018).

Whether mTORC2 assembly is regulated by growth factors is still debated (Jain et al., 2014; Wang et al., 2017). However, mTORC2 components are susceptible to posttranslational modifications (PTMs), which influence their incorporation into mTORC2. For example, TRAF2-mediated Lys63-linked polyubiquitination of mLST8 regulates its binding to mTOR complexes (Wang et al., 2017), and phosphorylation of RICTOR-Thr1695 promotes FBXW7-mediated degradation of RICTOR (Koo et al., 2015). However, it is unclear whether and how growth factors regulate enzymes controlling mTORC2-specific PTMs. In our study, we showed that mTORC2 assembly and consequent activity are regulated by the availability of growth factors, since growth factors stimulate *USP9X* expression and USP9X hydrolyzes ubiquitination on RICTOR Lys274 to promote its interaction with mTOR.

The mRNA and protein levels of Usp9x in mouse liver are quite variable between animals, possibly reflecting the dynamic alterations of protein expression in response to nutrient availability. To avoid misinterpretation of the data in the *in vivo Usp9x* knockdown experiment, we used more than 10 animals per group, which was sufficient to show significant decrease in mTORC2 substrate phosphorylation. Our abilities to make firm conclusions about the physiological importance of USP9X regulation of mTORC2 assembly was limited by the following issues. Deletion of *Usp9x* in mouse is embryonically lethal (Pantaleon et al., 2001), and we could not generate USP9X null cell lines (presumably because of this lethality). Thus, we were not able to address

Figure 4. Growth Factors Regulate USP9X Expression to Regulate Hepatic mTORC2 Signaling

(A) HeLa cells were starved in serum-free, amino-acids-free, Glc-free, or Hank's balanced salt solution (HBSS) medium for 8 h and lysed (n = 4).

(B and C) *USP9X*-Gluc-ON promoter HeLa cells were serum starved for 1 h (B; n = 3) or 18 h serum starved and refed with full media for 1 h (C; n = 6). Ratio of *Gaussia* luciferase/secreted alkaline phosphatase (SEAP).

(D) HeLa cells were serum starved for 18 h, refed with full media for 3 h, and then mRNA levels of *USP9X* and *GAPDH* were measured by RT-PCR (n = 5).

(E) HeLa cells were serum starved for 24 h followed by incubation in full media in the presence of 10 μM BMS-536924 or 1 μM Torin1 for 6 h (n = 5). One-way ANOVA ($p < 0.01$) with Tukey post hoc test ($p < 0.05$).

(F) Control and USP9X knockdown HeLa cells were starved in Earle's balanced salts solution (EBSS) for 5 h, refed with full media for 2 h, and lysed.

(G and H) Mice were fasted for 22 h, followed by free access to food for 2 h followed by fasting for another 22 h. The liver tissue samples were analyzed for protein levels (G) or *Usp9x* and *Gapdh* mRNA levels (H; one-tailed unpaired Student's t test).

(I and J) Male control and mice depleted of Usp9x for 5 days were fasted for 23 h followed by free access to food for 2 h. The liver tissue samples were analyzed; statistical analysis in (J), two-tailed unpaired Student's t test.

(K) Model proposed on how nutrient availability regulates USP9X levels to promote mTORC2 signaling. Presence of extracellular nutrients increase transcription of *USP9X* and increase USP9X levels. USP9X deubiquitinates RICTOR Lys274, causing its stabilization and promoting its binding to mTOR kinase. Increase in the mTORC2 assembly results in the increased mTOR activity toward its downstream targets.

For (A) and (E)–(I), protein phosphorylation and levels were determined by immunoblotting with the indicated antibodies. Mean ± SEM. Two-tailed paired Student's t test, if not stated otherwise, $^{*}p < 0.05$, $^{**}p < 0.01$, and $^{***}p < 0.001$. AU, arbitrary units.

how complete loss of USP9X affects mTORC2 integrity *in vivo* or in cell culture. Potentially, this issue could be addressed in future studies using conditional knockouts of *Usp9x* in mice (e.g., in the liver). We were also unable to assess mTORC2 integrity *in vivo*, due to lack of antibodies that could specifically immunoprecipitate endogenous mTOR complexes. It would be interesting to evaluate the changes in mTORC2 assembly under varying physiological conditions in liver, and also in other metabolically important tissues, using immunoprecipitation (IP) or alternative approaches.

In a healthy organism, mTORC2 signaling is crucial for whole-body metabolic homeostasis in response to changing nutrient availability. Aberrant insulin-mediated mTORC2 signaling in liver, muscle, and adipose tissue affects a broad spectrum of downstream targets controlling Glc and lipid homeostasis (Hagiwara et al., 2012; Kumar et al., 2008, 2010; Yuan et al., 2012), suggesting that mTORC2 dysregulation can contribute to human metabolic disorders. In cancer, aberrant activation of the PI3K/AKT/mTOR signaling pathway promotes cell survival and proliferation, with AKT being among the most commonly hyperactivated proteins in cancer, often correlated with increased levels of RICTOR (Kim et al., 2017), demonstrating the importance of tight regulation of mTORC2. Modulation of mTOR-RICTOR complex formation, for example, by inhibiting USP9X activity, may represent a promising therapeutic target in cancer research.

STAR★METHODS

Detailed methods are provided in the online version of this paper and include the following:

- KEY RESOURCES TABLE
- RESOURCE AVAILABILITY
  - Lead Contact
  - Materials Availability
  - Data and Code Availability
- EXPERIMENTAL MODEL AND SUBJECT DETAILS
  - Cell lines
  - Mice
- METHOD DETAILS
  - Cell culture and transfection
  - Plasmids, siRNA and shRNAs
  - Antibodies and reagents
  - Lentivirus production and cell infection
  - Transient siRNA knock down in mice, blood sampling and tissue isolation
  - RNA isolation and quantitative real time PCR
  - Luminescence assay
  - Immunoprecipitation and ubiquitination analysis
  - Proximity ligation assay
  - Western blot analysis
  - RICTOR purification and *in vitro* deubiquitination (DUB) assay
  - Mass spectrometry analysis for posttranslational modification sites
- QUANTIFICATION AND STATISTICAL ANALYSIS

SUPPLEMENTAL INFORMATION

Supplemental Information can be found online at https://doi.org/10.1016/j.celrep.2020.108564.

ACKNOWLEDGMENTS

We are grateful for funding from the UK Dementia Research Institute (funded by the MRC, Alzheimer's Research UK, and the Alzheimer's Society) (to D.C.R.), the Roger de Spoelberch Foundation (to D.C.R.), the European Molecular Biology Organisation (EMBO long-term fellowships ALTF 135-2016 and ALTF 1024-2016 to L.W. and S.M.H., respectively), and the Swedish Natural Research Council (VR) (to S.M.H.; reference 2016–06605). We thank So Jung Park for tissue preparation and Robin Antrobus and Jack Houghton at CIMR proteomics facility for mass spectrometry analysis.

AUTHOR CONTRIBUTIONS

L.W. and D.C.R. developed the study rationale. L.W. and D.C.R. wrote the manuscript with input from other authors. L.W. designed and performed most of the experiments, with help of S.M.S. F.H.S. performed mouse experiments with help of C.K. and H.K. S.M.H. purified RICTOR proteins. D.C.R. supervised the study.

DECLARATION OF INTERESTS

D.C.R. is a consultant for Aladdin Healthcare Technologies SE and Nido Biosciences. None of the other authors have any potential competing interests.

Received: May 5, 2020
Revised: October 14, 2020
Accepted: December 7, 2020
Published: December 29, 2020

REFERENCES

Agrawal, P., Chen, Y.T., Schilling, B., Gibson, B.W., and Hughes, R.E. (2012). Ubiquitin-specific peptidase 9, X-linked (USP9X) modulates activity of mammalian target of rapamycin (mTOR). J. Biol. Chem. *287*, 21164–21175.

Ashkenazi, A., Bento, C.F., Ricketts, T., Vicinanza, M., Siddiqi, F., Pavel, M., Squitieri, F., Hardenberg, M.C., Imarisio, S., Menzies, F.M., and Rubinsztein, D.C. (2017). Polyglutamine tracts regulate autophagy. Autophagy *13*, 1613–1614.

Aspernig, H., Heimbucher, T., Qi, W., Gangurde, D., Curic, S., Yan, Y., Donner von Gromoff, E., Baumeister, R., and Thien, A. (2019). Mitochondrial Perturbations Couple mTORC2 to Autophagy in C. elegans. Cell Rep. *29*, 1399–1409.e5.

Bridges, C.R., Tan, M.C., Premarathne, S., Nanayakkara, D., Bellette, B., Zencak, D., Domingo, D., Gecz, J., Murtaza, M., Jolly, L.A., and Wood, S.A. (2017). USP9X deubiquitylating enzyme maintains RAPTOR protein levels, mTORC1 signalling and proliferation in neural progenitors. Sci. Rep. *7*, 391.

Chen, X., Overstreet, E., Wood, S.A., and Fischer, J.A. (2000). On the conservation of function of the Drosophila fat facets deubiquitinating enzyme and Fam, its mouse homolog. Dev. Genes Evol. *210*, 603–610.

Chen, X., Liu, M., Tian, Y., Li, J., Qi, Y., Zhao, D., Wu, Z., Huang, M., Wong, C.C.L., Wang, H.W., et al. (2018). Cryo-EM structure of human mTOR complex 2. Cell Res. *28*, 518–528.

Ebner, M., Sinkovics, B., Szczygieł, M., Ribeiro, D.W., and Yudushkin, I. (2017). Localization of mTORC2 activity inside cells. J. Cell Biol. *216*, 343–353.

Facchinetti, V., Ouyang, W., Wei, H., Soto, N., Lazorchak, A., Gould, C., Lowry, C., Newton, A.C., Mao, Y., Miao, R.Q., et al. (2008). The mammalian target of rapamycin complex 2 controls folding and stability of Akt and protein kinase C. EMBO J. *27*, 1932–1943.

Frias, M.A., Thoreen, C.C., Jaffe, J.D., Schroder, W., Sculley, T., Carr, S.A., and Sabatini, D.M. (2006). mSin1 is necessary for Akt/PKB phosphorylation, and its isoforms define three distinct mTORC2s. Curr. Biol. *16*, 1865–1870.

Gan, X., Wang, J., Su, B., and Wu, D. (2011). Evidence for direct activation of mTORC2 kinase activity by phosphatidylinositol 3,4,5-trisphosphate. J. Biol. Chem. *286*, 10998–11002.

García-Martínez, J.M., and Alessi, D.R. (2008). mTOR complex 2 (mTORC2) controls hydrophobic motif phosphorylation and activation of serum- and glucocorticoid-induced protein kinase 1 (SGK1). Biochem. J. *416*, 375–385.

Glidden, E.J., Gray, L.G., Vemuru, S., Li, D., Harris, T.E., and Mayo, M.W. (2012). Multiple site acetylation of Rictor stimulates mammalian target of rapamycin complex 2 (mTORC2)-dependent phosphorylation of Akt protein. J. Biol. Chem. *287*, 581–588.

Guertin, D.A., Stevens, D.M., Thoreen, C.C., Burds, A.A., Kalaany, N.Y., Moffat, J., Brown, M., Fitzgerald, K.J., and Sabatini, D.M. (2006). Ablation in mice of the mTORC components raptor, rictor, or mLST8 reveals that mTORC2 is required for signaling to Akt-FOXO and PKCalpha, but not S6K1. Dev. Cell *11*, 859–871.

Hagiwara, A., Cornu, M., Cybulski, N., Polak, P., Betz, C., Trapani, F., Terracciano, L., Heim, M.H., Rüegg, M.A., and Hall, M.N. (2012). Hepatic mTORC2 activates glycolysis and lipogenesis through Akt, glucokinase, and SREBP1c. Cell Metab. *15*, 725–738.

Ikenoue, T., Inoki, K., Yang, Q., Zhou, X., and Guan, K.L. (2008). Essential function of TORC2 in PKC and Akt turn motif phosphorylation, maturation and signalling. EMBO J. *27*, 1919–1931.

Jacinto, E., Facchinetti, V., Liu, D., Soto, N., Wei, S., Jung, S.Y., Huang, Q., Qin, J., and Su, B. (2006). SIN1/MIP1 maintains rictor-mTOR complex integrity and regulates Akt phosphorylation and substrate specificity. Cell *127*, 125–137.

Jain, A., Arauz, E., Aggarwal, V., Ikon, N., Chen, J., and Ha, T. (2014). Stoichiometry and assembly of mTOR complexes revealed by single-molecule pulldown. Proc. Natl. Acad. Sci. USA *111*, 17833–17838.

Kim, J., and Guan, K.L. (2019). mTOR as a central hub of nutrient signalling and cell growth. Nat. Cell Biol. *21*, 63–71.

Kamitani, T., Kito, K., Nguyen, H.P., and Yeh, E.T. (1997). Characterization of NEDD8, a developmentally down-regulated ubiquitin-like protein. J Biol Chem *272*, 28557–28562.

Kim, W., Bennett, E.J., Huttlin, E.L., Guo, A., Li, J., Possemato, A., Sowa, M.E., Rad, R., Rush, J., Comb, M.J., et al. (2011). Systematic and quantitative assessment of the ubiquitin-modified proteome. Mol. Cell *44*, 325–340.

Kim, L.C., Cook, R.S., and Chen, J. (2017). mTORC1 and mTORC2 in cancer and the tumor microenvironment. Oncogene *36*, 2191–2201.

Koo, J., Wu, X., Mao, Z., Khuri, F.R., and Sun, S.Y. (2015). Rictor Undergoes Glycogen Synthase Kinase 3 (GSK3)-dependent, FBXW7-mediated Ubiquitination and Proteasomal Degradation. J. Biol. Chem. *290*, 14120–14129.

Kumar, A., Harris, T.E., Keller, S.R., Choi, K.M., Magnuson, M.A., and Lawrence, J.C., Jr. (2008). Muscle-specific deletion of rictor impairs insulin-stimulated glucose transport and enhances Basal glycogen synthase activity. Mol. Cell. Biol. *28*, 61–70.

Kumar, A., Lawrence, J.C., Jr., Jung, D.Y., Ko, H.J., Keller, S.R., Kim, J.K., Magnuson, M.A., and Harris, T.E. (2010). Fat cell-specific ablation of rictor in mice impairs insulin-regulated fat cell and whole-body glucose and lipid metabolism. Diabetes *59*, 1397–1406.

Liu, P., Gan, W., Chin, Y.R., Ogura, K., Guo, J., Zhang, J., Wang, B., Blenis, J., Cantley, L.C., Toker, A., et al. (2015). PtdIns(3,4,5)P3-Dependent Activation of the mTORC2 Kinase Complex. Cancer Discov. *5*, 1194–1209.

Mammucari, C., Milan, G., Romanello, V., Masiero, E., Rudolf, R., Del Piccolo, P., Burden, S.J., Di Lisi, R., Sandri, C., Zhao, J., et al. (2007). FoxO3 controls autophagy in skeletal muscle in vivo. Cell Metab. *6*, 458–471.

Metzakopian, E., Strong, A., Iyer, V., Hodgkins, A., Tzelepis, K., Antunes, L., Friedrich, M.J., Kang, Q., Davidson, T., Lamberth, J., et al. (2017). Enhancing the genome editing toolbox: genome wide CRISPR arrayed libraries. Sci. Rep. *7*, 2244.

Murtaza, M., Jolly, L.A., Gecz, J., and Wood, S.A. (2015). La FAM fatale: USP9X in development and disease. Cell. Mol. Life Sci. *72*, 2075–2089.

Oh, W.J., and Jacinto, E. (2011). mTOR complex 2 signaling and functions. Cell Cycle *10*, 2305–2316.

Pantaleon, M., Kanai-Azuma, M., Mattick, J.S., Kaibuchi, K., Kaye, P.L., and Wood, S.A. (2001). FAM deubiquitylating enzyme is essential for preimplantation mouse embryo development. Mech. Dev. *109*, 151–160.

Paudel, P., Zhang, Q., Leung, C., Greenberg, H.C., Guo, Y., Chern, Y.H., Dong, A., Li, Y., Vedadi, M., Zhuang, Z., and Tong, Y. (2019). Crystal structure and activity-based labeling reveal the mechanisms for linkage-specific substrate recognition by deubiquitinase USP9X. Proc. Natl. Acad. Sci. USA *116*, 7288–7297.

Peterson, L.F., Sun, H., Liu, Y., Potu, H., Kandarpa, M., Ermann, M., Courtney, S.M., Young, M., Showalter, H.D., Sun, D., et al. (2015). Targeting deubiquitinase activity with a novel small-molecule inhibitor as therapy for B-cell malignancies. Blood *125*, 3588–3597.

Renna, M., Bento, C.F., Fleming, A., Menzies, F.M., Siddiqi, F.H., Ravikumar, B., Puri, C., Garcia-Arencibia, M., Sadiq, O., Corrochano, S., et al. (2013). IGF-1 receptor antagonism inhibits autophagy. Hum. Mol. Genet. *22*, 4528–4544.

Sarbassov, D.D., Ali, S.M., Kim, D.H., Guertin, D.A., Latek, R.R., Erdjument-Bromage, H., Tempst, P., and Sabatini, D.M. (2004). Rictor, a novel binding partner of mTOR, defines a rapamycin-insensitive and raptor-independent pathway that regulates the cytoskeleton. Curr. Biol. *14*, 1296–1302.

Sarbassov, D.D., Guertin, D.A., Ali, S.M., and Sabatini, D.M. (2005). Phosphorylation and regulation of Akt/PKB by the rictor-mTOR complex. Science *307*, 1098–1101.

Saxton, R.A., and Sabatini, D.M. (2017). mTOR Signaling in Growth, Metabolism, and Disease. Cell *169*, 361–371.

Skowyra, A., Allan, L.A., Saurin, A.T., and Clarke, P.R. (2018). USP9X Limits Mitotic Checkpoint Complex Turnover to Strengthen the Spindle Assembly Checkpoint and Guard against Chromosomal Instability. Cell Rep. *23*, 852–865.

Sonenberg, N., and Hinnebusch, A.G. (2009). Regulation of translation initiation in eukaryotes: mechanisms and biological targets. Cell *136*, 731–745.

Stuttfeld, E., Aylett, C.H., Imseng, S., Boehringer, D., Scaiola, A., Sauer, E., Hall, M.N., Maier, T., and Ban, N. (2018). Architecture of the human mTORC2 core complex. eLife *7*, e33101.

Vlahakis, A., Graef, M., Nunnari, J., and Powers, T. (2014). TOR complex 2-Ypk1 signaling is an essential positive regulator of the general amino acid control response and autophagy. Proc. Natl. Acad. Sci. USA *111*, 10586–10591.

Wang, B., Jie, Z., Joo, D., Ordureau, A., Liu, P., Gan, W., Guo, J., Zhang, J., North, B.J., Dai, X., et al. (2017). TRAF2 and OTUD7B govern a ubiquitin-dependent switch that regulates mTORC2 signalling. Nature *545*, 365–369.

Wu, L., and Belasco, J.G. (2008). Let me count the ways: mechanisms of gene regulation by miRNAs and siRNAs. Mol. Cell *29*, 1–7.

Xu, W., Hua, H., Chiu, Y.H., Li, G., Zhi, H., Yu, Z., Ren, F., Luo, Y., and Cui, W. (2019). CD146 Regulates Growth Factor-Induced mTORC2 Activity Independent of the PI3K and mTORC1 Pathways. Cell Rep. *29*, 1311–1322.e5.

Yang, Q., Inoki, K., Ikenoue, T., and Guan, K.L. (2006). Identification of Sin1 as an essential TORC2 component required for complex formation and kinase activity. Genes Dev. *20*, 2820–2832.

Young, J.A., Sermwittayawong, D., Kim, H.J., Nandu, S., An, N., Erdjument-Bromage, H., Tempst, P., Coscoy, L., and Winoto, A. (2011). Fas-associated death domain (FADD) and the E3 ubiquitin-protein ligase TRIM21 interact to negatively regulate virus-induced interferon production. J. Biol. Chem. *286*, 6521–6531.

Yuan, M., Pino, E., Wu, L., Kacergis, M., and Soukas, A.A. (2012). Identification of Akt-independent regulation of hepatic lipogenesis by mammalian target of rapamycin (mTOR) complex 2. J. Biol. Chem. *287*, 29579–29588.

Zeng, Y., Yi, R., and Cullen, B.R. (2003). MicroRNAs and small interfering RNAs can inhibit mRNA expression by similar mechanisms. Proc. Natl. Acad. Sci. USA *100*, 9779–9784.

Zinzalla, V., Stracka, D., Oppliger, W., and Hall, M.N. (2011). Activation of mTORC2 by association with the ribosome. Cell *144*, 757–768.

STAR★METHODS

KEY RESOURCES TABLE

REAGENT or RESOURCE	SOURCE	IDENTIFIER
Antibodies		
mouse anti-Flag M2	Sigma Aldrich	Cat#F3165
rabbit anti-Actin	Sigma Aldrich	Cat#A2066
mouse anti-a-Tubulin	Sigma Aldrich	Cat#T9026
mouse anti-HA.11 clone 16B12	Covance	Cat#MMS-101P
rabbit anti-USP9X	Abcam	Cat#ab19879
rabbit anti-USP9X	Bethyl	Cat#A301-351A
rabbit anti-RICTOR	Abcam	Cat#ab70374
rabbit anti-RICTOR	Bethyl	Cat#A300-458A
mouse anti-RICTOR	Nouvus	Cat#NBP1-51645SS
rabbit anti-mTOR	Cell Signaling	Cat#2972
rabbit anti-mTOR	Cell Signaling	Cat#2983
rabbit anti-phospho-p70 S6kinase (Thr389)	Cell Signaling	Cat##9234
rabbit anti-total p70 S6 kinase	Cell Signaling	Cat#9202
rabbit anti-phospho-4E-BP1(Thr37/46)	Cell Signaling	Cat#9459
rabbit anti-4E-BP1	Cell Signaling	Cat#9452
rabbit anti-RAPTOR	Cell Signaling	Cat#2280
rabbit anti-mLST8	Cell Signaling	Cat#3274
rabbit anti-mSIN1	Cell Signaling	Cat#D7GaA
rabbit anti-phospho-PKCα/βII(Thr638/641)	Cell Signaling	Cat#9375
rabbit anti-PKCα	Cell Signaling	Cat#2056
rabbit anti-AKT	Cell Signaling	Cat#C67E7
mouse anti-AKT	Cell Signaling	Cat#9272
mouse anti-AKT1	Cell Signaling	Cat#2H10
rabbit anti-phospho-AKT(Ser473)	Cell Signaling	Cat#4060
rabbit anti-phospho-AKT(Thr450)	Cell Signaling	Cat#9262
rabbit anti-phospho-AKT(Thr308)	Cell Signaling	Cat#9275
rabbit anti-Fox03a	Cell Signaling	Cat#2497
rabbit anti-phospho-Fox01(Thr24)/Fox03a(Thr32)	Cell Signaling	Cat#9464
rabbit anti-K63-linkage specific polyubiquitin(D7A11)	Cell Signaling	Cat#5621
rabbit anti-K48-linkage specific polyubiquitin(D9D5)	Cell Signaling	Cat#8081
rabbit anti-PARP	Cell Signaling	Cat#46D11
rabbit anti-phospho-GSK-3β(Ser9)	Cell Signaling	Cat#9336
rabbit anti-ACC-S79	Cell Signaling	Cat#11818
rabbit anti-MCL1	Abcam	Cat##ab32087
rabbit anti-GFP	Abcam	Cat#6556
mouse anti-myc tag	Abcam	Cat#ab206486
rabbit anti-LC3B	Abcam	Cat#ab192890
rabbit anti-calnexin	Abcam	Cat#ab133615
mouse anti-GAPDH	Abcam	Cat#ab8245
Chemicals, Peptides, and Recombinant Proteins		
BafA1	Enzo	Cat#BML-CM110
MG132 (Z-Leu-Leu-Leu-al)	Sigma Aldrich	Cat#C2211
EOAI3402143 (G9)	Glixx Laboratories Inc	Cat#GLXC-09781

(*Continued on next page*)

Continued

REAGENT or RESOURCE	SOURCE	IDENTIFIER
Torin1	Tocris	Cat#4247
BMS536924	Tocris	Cat#4774
USP9X-His_6	BostonBiochem	Cat#E-552
Critical Commercial Assays		
Secrete-Pair Dual Luminescence Assay Kit	Genecopoeia	cat#LF031
Duolink *In Situ* Detection Assay	Sigma Aldrich	cat# DUO92008-30RXN
Experimental Models: Cell Lines		
HeLa	ATCC	Cat#CCL-2
SH-SY5Y	ECACC	Cat#94030304
HepG2	ECACC	Cat#85011430
MEF	gift from Prof N. Mizushima (University of Tokyo)	N/A
HEK293FT	Invitrogen	Cat##R70007
HeLa with dox-inducible Flag-USP9X WT	Skowyra et al., 2018	N/A
HeLa with dox-inducible Flag-USP9X-CD mutant	Skowyra et al., 2018	N/A
USP9X-Gluc-ON Promoter HeLa stable cell line	This paper	N/A
HEK293FT control non-targeting gRNA cell line	This paper	N/A
HEK293FT RICTOR knockout cell line	This paper	N/A
Expi293F suspension cells	GIBCO	Cat#A14527
Experimental Models: Organisms/Strains		
Mouse: C57BL/6J	The Jackson Laboratory	stock#000664
Oligonucleotides		
siRNA targeting sequence USP9X oligo 6: 5′-AGAAAUCGCUGGUAUAAAAU-3′	Dharmacon	Cat#J-006099-06
siRNA targeting sequence USP9X oligo 7: 5′-ACACGAUGCUUUAGAAUUU-3′	Dharmacon	Cat#J-006099-07
siRNA targeting sequence USP9X oligo 8: 5′-GUACGACGAUGUAUUCUCA-3′	Dharmacon	Cat#J-006099-08
siRNA targeting sequence USP9X oligo 9: 5′-GAAAUAACUUCCUACCGAA-3′	Dharmacon	Cat#J-006099-09
In vivo pre-designed siRNA targeting mouse USP9X: 5′- GGAUUACAGCUGGUAUUCAtt-3′	Ambion	Cat#s75828
Forward primer used for RICTOR mutagenesis: 5′-CTGAAGGACAGCTCCGAGAAGACAGAGAAGC-3′	This paper	N/A
Reverse primer used for RICTOR mutagenesis: 5′-GCTTCTCTGTCTTCTCGGAGCTGTCCTTCAG-3′	This paper	N/A
Forward RT-PCR USP9X_mouse: 5′- AGTCAAAGTCAGCGAAGTCCC-3′	This paper	N/A
Reverse RT-PCR USP9X_mouse: 5′- CCAGTCTCACAGTTTGTGGGT-3′	This paper	N/A
Forward RT-PCR USP9X_human: 5′- TGTTACACCCACTGCACTCT-3′	This paper	N/A
Reverse RT-PCR USP9X_human: 5′-TGACATGGATGGGCTCTGTT-3′	This paper	N/A
Forward RT-PCR GAPDH_mouse: 5′- TGCACCACCAACTGCTTAGC	This paper	N/A
Reverse RT-PCR GAPDH_mouse: 5′- GGCATGGACTGTGGTCATGAG	This paper	N/A
Forward RT-PCR GAPDH_human: 5′-CCACTAGGCCGCTCACTGTTC-3′	This paper	N/A
Reverse RT-PCR GAPDH_human: 5′-ACCAAATCCGTTGACTCCGAC-3′	This paper	N/A

(*Continued on next page*)

Continued

REAGENT or RESOURCE	SOURCE	IDENTIFIER
Recombinant DNA		
myc-RICTOR	Sarbassov et al., 2004	Addgene #11367
myc-mTOR	Sarbassov et al., 2004	Addgene #1861
pCI-His-hUbi	Young et al., 2011	Addgene #31815
N1-mSin1.1-GFP	Ebner et al., 2017	Addgene #72907
N1-mSin1.2-GFP	Ebner et al., 2017	Addgene #72908
N1-mSin1.5-GFP	Ebner et al., 2017	Addgene #72909
HA-ubiquitin	(Kamitani et al., 1997)	Addgene #18712
pEGFP-C1-USP9X	MRC PPU Reagents and Services	Cat#DU10181
pcDNA3.1-myc-His	Invitrogen	Cat#V80020
His-Ub(K63only)	Wang et al., 2017	N/A
His-Ub(K48only)	Wang et al., 2017	N/A
USP9X-Gluc-ON Promoter Reporter construct	Genecopoeia	Cat#HPRM32942-LVPG04
myc-RICTOR-K274R	This paper	N/A
pLKO.1 shRNA empty vector control	The RNAi Consortium (TRC)	Cat#RHS4080
pLKO.1 shRNA Usp9x (Clone ID: TRCN0000030759)	The RNAi Consortium (TRC)	Cat#RMM3981-201761066
pcDNA3-HA/FLAG-RICTOR	Glidden et al., 2012	N/A
pcDNA3-HA/FLAG-RICTOR-K274R	This paper	N/A
pKLV-PB-U6gRNA(*Bbs*I)-PGKpuro2ABFP (Lenti-PB) [gRNA RICTOR vector]	Metzakopian et al., 2017	N/A
pKLV-PB-U6gRNA(*Bbs*I)-PGKpuro2ABFP (Lenti-PB) [Non-targeting gRNA vector]	Metzakopian et al., 2017	N/A
pKLV-Cas9 vector	Metzakopian et al., 2017	N/A
Software and Algorithms		
Prism v7	GraphPad	N/A
ZEN Black	Carl Zeiss Microscopy	N/A
Image Studio Lite	LI-COR, Inc	N/A
ImageJ	National Institute of Health, USA	N/A
Excel	Microsoft Office	N/A

RESOURCE AVAILABILITY

Lead Contact

Further information and requests for resources and reagents should be directed to and will be fulfilled by the Lead Contact, David C Rubinsztein (dcr1000@cam.ac.uk).

Materials Availability

All unique/stable reagents generated in this study are available from the Lead Contact with a completed Materials Transfer Agreement.

Data and Code Availability

This study did not generate datasets or code.

EXPERIMENTAL MODEL AND SUBJECT DETAILS

Cell lines

Human cervical cancer (HeLa), human neuroblastoma (SH-SY5Y), human embryonic kidney 293 (HEK293FT), human liver cancer (HepG2) cell lines and mouse embryonic fibroblasts (MEFs) were cultured in Dulbecco's modified Eagle's medium (for HeLa, HEK293FT and MEFs; Sigma#D6548) or in RPMI (for HepG2; Sigma#1640) or in DMEM/F12 (for SH-SY5Y; Sigma#6421) supplemented with 2 mM L-glutamine, 100 U/ml Penicillin/Streptomycin and 10% Fetal Bovine Serum (FBS) in 5% CO_2 at 37°C. HeLa

dox-inducible Flag-USP9X WT and catalytically dead CD mutant (C1566A) were generous gifts from A. Saurin (Jacqui Wood Cancer Centre, University of Dundee) (Skowyra et al., 2018). *USP9X*-Gluc-ON Promoter HeLa stable cell line was generated by transfection with lentiviral *USP9X*-Gluc-ON Promoter Reporter construct (HPRM32942-LVPG04; Genecopoeia). All the cell lines were routinely tested for mycoplasma contamination.

HEK293FT RICTOR knockout cell line was generated using CRISPR/Cas9. Briefly, pre-designed gRNA RICTOR vector (sequence: F|CACCGAACTGTCTTGGAACCTCCCGT; R|TAAAACGGGAGGTTCCAAGACAGTTC) or non-targeting gRNA vector control together with Cas9 expressing vector (kind gifts from E. Metzakopian, UK DRI University of Cambridge) (Metzakopian et al., 2017) were transiently transfected into HEK293FT cells. 24 h after transfection, medium was replaced with media containing 2 μg/ml puromycin and kept for three days prior to single-cell sorting into 96-well plates using FACS. Clones were expanded and tested for the level of RICTOR.

Mice

Mouse studies and procedures were performed under the jurisdiction of UK Home Office Project and Personal animal licenses and with local Ethics Committee approval. Mice were housed in individually ventilated cages with free access to standard animal food chow and water, in a climate-controlled room with a 12 h light/dark cycle, except when subjected to starvation-refeeding protocols specifically mentioned below. C57BL/6 J (Jackson Laboratories) male and female mice, age between 7-10 weeks and weighing approximately 20-30 g were used.

METHOD DETAILS

Cell culture and transfection

For starvation, cells were washed with PBS twice and cultured in FBS-free DMEM or *Hanks' Balanced Salt Solution* (HBSS) medium (Invitrogen). For glucose starvation, cells were washed with PBS and cultured in DMEM without glucose (GIBCO#11966025) supplemented with 10% FBS and sodium pyruvate. For amino acids starvation, cells were washed with PBS and cultured in DMEM supplemented with 10% dialyzed FBS (GIBCO#A3382001). Cell transfection was performed with TransIT 2020 (for pDNA; Mirus) or Lipofectamine 2000 reagents (for siRNA; Invitrogen) in GIBCOOpti-MEM I Reduced Medium (GIBCO#11524456) using the manufacturers' protocols. Final siRNA concentrations of 20–50 nM was used for silencing for 3-5 days.

Plasmids, siRNA and shRNAs

The following expression vectors were used: myc-RICTOR (#11367) (Sarbassov et al., 2004), myc-mTOR (#1861) (Jain et al., 2014), pCI-His-hUbi (#31815), N1-mSIN1.1-GFP (#72907), N1-mSIN1.2-GFP (#72908), N1-mSIN1.5-GFP (#72909) (Ebner et al., 2017), HA-ubiquitin (#18712) from Addgene (Young et al., 2011); pEGFP-C1-USP9X (MRC PPU Reagents and Services#DU10181): as a control empty pEGFP and pcDNA3.1-myc-His (Invitrogen) were used. His-UB(K63only) and His-UB(K48only) were kindly provided by Wenyi Wei (Beth Israel Deaconess Medical Center, Harvard Medical School) (Wang et al., 2017). pcDNA3-HA/FLAG-RICTOR was kindly provided by Marty W. Mayo (University of Virginia) (Glidden et al., 2012). The lentiviral *USP9X*-Gluc-ON Promoter Reporter construct (HPRM32942-LVPG04) was purchased from Genecopoeia. The myc-RICTOR-K274R and pcDNA3-HA/FLAG-RICTOR-K274R were constructed using Site-Directed Mutagenesis Kit (Stratagene) following manufacturer's instructions, using following primers: 5′-CTGAAGGACAGCTCCGAGAAGACAGAGAAGC-3′ and 5′-GCTTCTCTGTCTTCTCGGAGCTGTCCTTCAG-3′. Pre-designed siRNAs (ON-TARGETplus SMARTpool and/or set of deconvoluted oligos) from GE Healthcare Dharmacon): control non-targeting siRNA (#D-001810-10); *USP9X* Smart Pool (#L-006099-00-0005), *USP9X* oligo 6: 5′-AGAAAUCGCUGGUAUAAAAU-3′ (#J-006099-06); *USP9X* oligo 7: 5′-ACACGAUGCUUUAGAAUUU-3′ (#J-006099-07); *USP9X* oligo 8: 5′-GUACGACGAUGUAUUCUCA-3′(#J-006099-08); *USP9X* oligo 9: 5′-GAAAUAACUUCCUACCGAA-3′(#J-006099-09); *RICTOR* Smart Pool (#L-006099-00-0005). Pre-designed pLKO.1 shRNAs vectors were purchased from The RNAi Consortium (TRC): empty vector control (#RHS4080), mouse *Usp9x* (Clone ID: TRCN0000030759, #RMM3981-201761066). *In vivo* pre-designed siRNA targeting mouse *Usp9x*: 5′- GGAUUACAGCUGGUAUUCAtt-3′ (#s75828) and control siRNA (#4457289) was purchased from Ambion.

Antibodies and reagents

The antibodies used were as follows: mouse anti-Flag M2 (#F3165), rabbit anti-Actin (#A2066) and mouse anti-a-Tubulin (#T9026) from Sigma Aldrich; mouse anti-HA.11 clone 16B12 (#MMS-101P, Covance), rabbit anti-USP9X (Abcam#ab19879 for western blot; Bethyl#A301-351A for endogenous IP); rabbit RICTOR (Bethyl#A300-458A for endogenous IP; Abcam#ab70374 for western blot); mouse anti-RICTOR (Nouvus#NBP1-51645SS for PLA assay); rabbit anti-mTOR (#2972 for western blot; #2983 for PLA assay), rabbit anti-phospho-p70 S6kinase (Thr389; #9234), anti-total p70 S6kinase (#9202), rabbit anti-phospho-4E-BP1 (Thr37/46; #9459), rabbit anti-4E-BP1 (#9452), rabbit anti-RAPTOR (#2280), rabbit anti-mLST8 (#3274), rabbit anti-mSIN1 (#D7GaA), rabbit anti-phospho-PKCα/βII(Thr638/641; #9375), rabbit anti-PKCα (#2056), rabbit anti-AKT (#C67E7), mouse anti-AKT (#9272), mouse anti-AKT1, rabbit anti-phospho-AKT-Ser473 (#4060), rabbit anti-phospho-AKT-Thr450 (#9262); rabbit anti-phospho-AKT-Thr308 (#9275); rabbit anti-FOX03a (#2497); rabbit anti-phospho-FOX01(Thr24)/FOX03a(Thr32) (#9464), rabbit anti-K63-linkage specific polyubiquitin (D7A11#5621), rabbit anti-K48-linkage specific polyubiquitin (D9D5#8081), rabbit anti-PARP, rabbit anti-phospho-GSK-3β-Ser9

(#9336), rabbit anti-ACC-S79(#11818S) from Cell Signaling; rabbit anti-MCL1 (Abcam#ab32087); rabbit anti-GFP (Abcam#6556); mouse anti-myc tag (Abcam#ab206486), rabbit anti-LC3B (Abcam#ab192890); rabbit anti-CALNEXIN (Abcam#ab133615), mouse anti-GAPDH (Abcam#ab8245). Drug treatment used include: BafA1 (Enzo, BML-CM110), MG132 (Z-Leu-Leu-Leu-al; Sigma Aldrich#C2211), EOAI3402143 (referred to as G9; Glixx Laboratories Inc#GLXC-09781), Insulin (Sigma), Torin1 (TOCRIS#4247), Cycloheximide (Sigma) BMS536924 (TOCRIS#4774), Doxycycline (Sigma), Puromycin (GIBCO).

Lentivirus production and cell infection

shRNA and *USP9X*-Gluc-ON Promoter Reporter lentiviral particles were produced and transduced following The RNAi Consortium (TRC) protocols. Briefly, HEK293FT packaging cells were transfected with a mix of packaging vector (psPAX2), envelope vector (pMD2.G) and lentiviral expression vector. TransIT-LT1 (Mirus) was used as transfection reagent. Cell culture medium was harvested after 48 h and viral preps were then concentrated by centrifugation at 160,100 g for 90 min. Depending on the cell type, different viral titers were added to the cells in the presence of 4mg/ml polybrene (Sigma Aldrich) and were incubated overnight. After 24 h, medium was replaced by full medium and cells were further incubated in the presence of selection antibiotic (HeLa and MEFs: 1-3 μg/ml puromycin).

Transient siRNA knock down in mice, blood sampling and tissue isolation

For 46 h food deprivation experiment, C57BL/6 J male and female mice (age 10 weeks) were deprived of food for 22 h, followed by 2 h feeding period and again starvation for next 23 h. For 22 h food deprivation experiment, C57BL/6 J female mice (age 7-8 weeks) were deprived of food for 22 h. After starvation, the mice were sacrificed and liver tissues were collected. Mice had free access to water throughout the procedure. Mice were weighed before and after food deprivation and feeding period to make sure that total body weight loss is not more than 15%. Tissues were stored on dry ice for western blot analysis or mRNA analysis. *In vivo* siRNA knockdown experiment was performed as in Ashkenazi et al. (2017). Briefly, C57BL/6J male and female mice (Jackson Laboratories, age 8-9 weeks, weighing approx. 20-30 g), were depleted of Usp9x in the liver using the ThermoFisher Invivofectamine 3.0 system. The siRNA duplex solution and the preparation of the final injection solution were prepared according to the manufacturer's protocol. Briefly, siRNA (control siRNA#4457289; *Usp9x* siRNA#4457308) was mixed with the complexation buffer and then the Invivofectamine 3.0 reagent (ThermoFisher#IVF3005). The *Usp9x* siRNA was an Ambion pre-designed sequence: sense (5–3): GGAUUACAGCUGGUAUUCAtt; antisense (5–3): UGAAUACCAGCUGUAAUCCtc. The solution was vortexed, incubated at 50 °C for 30 min and then diluted in PBS. The solution was stored at 4 °C and subsequently up to 100 μl was injected into the lateral caudal vein at a final concentration of 2 mg kg–1 body weight. Mice were monitored for any adverse side effects briefly after injection (with none observed). Mice were randomly selected for injection with control or targeting siRNA and were matched by weight. The knockdown was left for 5 days. On the fifth day, a blood sample (100- 120 μl) was collected from the saphenous vein from all mice for basal levels of glucose, insulin and liver function analysis from control and knockdown mice. After blood sampling, the mice were deprived of food for a total period of 23 h with free access to water throughout the procedure. On the sixth day, after 23 h of food deprivation, mice were refed for 2 h. After 2 h refeeding, a terminal blood sample and liver tissues were collected from this group, as described above. Blood samples were sent to the core biochemical assay laboratory (CBAL, Cambridge University Hospital) for analysis. Various tissues from C57BL/6J mice (male, age 10 weeks) and also from above experiments were homogenized and resuspended in RIPA lysis buffer and proceeded as described in western blot analysis section.

RNA isolation and quantitative real time PCR

HeLa cells were deprived of FBS for 24 h and refed with full media containing FBS for 3 h. Total RNA was isolated using TRIzol reagent (Invitrogen#15596018), according to the manufacturer's protocol. The RNA sample was then treated with DNase I Amplification Grade (Invitrogen#18068-015) to remove any contaminating genomic DNA, followed by reverse transcription into cDNA with SuperScript III First Strand Synthesis System for RT-PCR (Invitrogen#1880-051). From mouse liver tissue, RNA was isolated as follows: approximately 100 mg of tissue was homogenized in 1 mL of TRIzol reagent and further treated according to manufacturer's protocol. After the step of chloroform centrifugation, samples were mixed with 100% ethanol to obtain 70% mixture and RNA purification was continued using PureLink RNA Mini Kit (Invitrogen#12183020) together with PureLink DNase Set (Invitrogen). The synthesized cDNA was mixed with primers and SYBR Green PCR Master Mix (Applied Biosystems#4309155) and processed by real time qPCR using a 7900 Fast Real-time PCR System (Applied Biosystems). The mRNA quantification of the target gene was based on the ΔΔCT method and the expression levels were plotted relative to GAPDH mRNA. Primers sequences in the Key Resource Table.

Luminescence assay

USP9X promoter activity was measured using Secrete-Pair Dual Luminescence Assay Kit (Genecopoeia #LF031) which allows one to analyze the activities of *Gaussia* Luciferase (GLuc) and Secreted Alkaline Phosphatase (SEAP) in the cell culture media. The *USP9X* promoter controls GLuc reporter gene expression, while SEAP is controlled by a cytomegalovirus (CMV) promoter. SEAP expression was used as a normalization factor. Briefly, HeLa cells containing *USP9X*-Gluc-ON Promoter Reporter construct were deprived of FBS for 24 h and refed with full media containing FBS for 1-6 h. Culture media was collected and luminescence was measured by Tecan Microplate Reader Spark®, according to manufacturer's protocols. The ratio of luminescence intensities of GLuc over SEAP was calculated for each sample.

Immunoprecipitation and ubiquitination analysis

Cells in 100 mm dishes were washed with PBS and lysed in ice-cold buffer. When analyzing mTOR complex formation, cells were lysed using CHAPS buffer [40 mM Tris pH 7.5, 120 mM NaCl, 1 mM EDTA, 0.3% CHAPS, protease inhibitors (Roche)] to preserve mTOR complex integrity. When analyzing RICTOR K-linkage ubiquitination, cells were lysed in Triton buffer [50 mM Tris pH 7.5, 250mM NaCl, 1% Triton X-100, protease inhibitors (Roche)]. When analyzing RICTOR-USP9X interactions, cells were lysed in NP-40 buffer [0.5% NP-40, 50 mM Tris pH 7.5, 150 mM NaCl, protease inhibitors (Roche)]. Lysates were incubated for 30 min on ice, followed by centrifugation at 16,100 g for 10 min, 4°C. Supernatants were incubated with primary antibodies overnight at 4°C, followed by incubation with Dynabeads Protein G (Invitrogen) for 2 h at 4°C or with GFP-Trap (ChromoTek# gtma-100) or myc-TRAP (ChromoTek#ytma-100), according to manufacturer's instructions. Bound material was washed three times with lysis buffer, followed by single wash with detergent-free buffer. When analyzing RICTOR ubiquitination under denaturing conditions, cells were lysed in 6 M guanidine-HCl, 100 mM Na_2HPO_4/NaH_2PO_4, 10 mM Tris pH 7.5, 20 mM Imidazole pH 8.0, 0.1% Triton X-100 and briefly sonicated. The polyubiquitinated proteins were purified by incubation with Ni-NTA agarose (QIAGEN) for 2 h at room temperature. Bound material was washed three times with 8 M Urea, 100 mM Na_2HPO_4/NaH_2PO_4, 10 mM Tris pH 7.5, 20 mM Imidazole pH 8.0 and eluted by incubating in 2x Laemmli buffer at 100°C for 10 min.

Proximity ligation assay

The proximity ligation assay kit was used according to manufacturer's instructions (Sigma Aldrich). Briefly, cells growing on coverslips were fixed in 4% paraformaldehyde in PBS for 10 min, permeabilized with 0.1% Triton X-100 in PBS for 5 min and blocked with the supplied blocking buffer. Subsequently, cells were incubated with anti-mTOR and anti-RICTOR (1:400) antibodies for 90 min at room temperature, followed by incubation with secondary antibodies conjugated to oligonucleotide primers (proximity ligation assay probes: MINUS and PLUS) for 1 h at 37°C. The primers were then ligated for 30 min at 37°C and followed by amplification for 100 min at 37°C. Coverslips were mounted on slides and imaged by LSM880 Confocal Microscope (Zeiss).

Western blot analysis

Cells were washed with ice-cold PBS and lysed with RIPA buffer [50 mM Tris-HCl pH 7.4, 150 mM NaCl, 1% Triton X-100, 0.5% sodium deoxycholatemonohydrate, 0.1% SDS, supplemented with protease (Roche) and phosphatase inhibitors cocktails (Sigma Aldrich)]. Cells were incubated on ice for 30 min. Mice tissue samples were lysed in RIPA buffer, centrifuged at 16,100 g for 10 min and the protein concentration of supernatants was determined using a DC Protein Assay (Bio-Rad). Tissue and cell lysates were then mixed with 2x Laemmli buffer with β-mercaptoethanol, boiled at 100°C for 5 min and resolved by SDS–PAGE and transferred onto polyvinylidene fluoride (PVDF) membranes. The membranes were blocked with 5% nonfat milk or 3% BSA in PBS, incubated with primary antibodies overnight, followed by HRP-conjugated (GE Healthcare) or DyLight Fluors-conjugated (Invitrogen) secondary antibodies. Immunoreactive bands were visualized with an ECL detection kit (Pierce, Thermo Scientific) in Bio-Rad ChemiDoc Imager or with direct infrared fluorescence detection using LICOR-Odyssey apparatus. Densitometric analysis on the immunoblots was performed using ImageJ program or IMAGE STUDIO Lite software. Western blots presented in each figure are representative of at least three biological replicates.

RICTOR purification and *in vitro* deubiquitination (DUB) assay

Expi293F suspension cells were grown to $2.5x10^6$ cells/mL in 500 mL of Expi293 Expression Medium (GIBCO). Cells were then transfected with 0,7 mg of FLAG-RICTOR and 2,1 mg Polyethylenimine 40K (Polysciences, Inc). On the day after transfection, culture was expanded to 1 L, and 3.3 mM valproic acid (Sigma) and 10 mg/mL Penicillin/Streptomycin (Sigma) was added. On day 2 post transfection, cells were treated with 5 μM MG132 and 5 μM USP9X inhibitor G9 (Glixx Laboratories) for 4 h before lysis. Cells were then collected, and lysed by homogenization in 80 mL buffer A (50 mM HEPES pH 8.0; 200 mM NaCl; 5% glycerol; protease inhibitors) with 0.1% CHAPS. Lysates were clarified by centrifugation at 100 000xg for 20 min and incubated with 1.5 mL packed agarose M2 anti-FLAG resin (Sigma) for 3 h at 4°C. Resin was transferred to a gravity flow column and washed 10X with buffer A (200 mM NaCl) and 2X in buffer A (50 mM NaCl). Proteins were eluted in fractions by incubation (4x60 min) with buffer A (50 mM NaCl) containing 150 ng/μl 3XFLAG peptides (Sigma). Purified proteins were analyzed on gels together with BSA standard to determine protein concentration and verified by western blot with antibodies against FLAG and RICTOR. *In vitro* assay was performed using 0.6 μg of purified RICTOR-FLAG and 1 μM USP9X-His_6 (BostonBiochem#E-552) in a buffer A with 50 mM NaCl and 5 mM DTT at 37°C for 5 h. Reaction was quenched by adding 2x Leammli buffer with β-mercaptoethanol.

Mass spectrometry analysis for posttranslational modification sites

Samples were reduced, alkylated and digested on-bead using trypsin. The resulting peptides were analyzed by LC-MSMS using a Thermo Q Exactive Pluss coupled to an Ultimate 3000 RSLC nano UHPLC equipped with a 100 μm ID x 2 cm Acclaim PepMap Precolumn (Thermo Fisher Scientific) and a 75 μm ID x 50 cm, 2 μm particle Acclaim PepMap RSLC analytical column. Loading solvent was 0.1% FA with analytical solvents A: 0.1% FA and B: 80% MeCN + 0.1% FA. Samples were loaded at 5 μl/min loading solvent for 5 min before beginning the analytical gradient. The analytical gradient was 3%–10% B over 2 min rising to 40% B by 57 min and 95% B by 59 min followed by a 5 min wash at 95% B and equilibration at 3% solvent B for 15 min. Columns were held at 40°C. Data were acquired in a DDA fashion with the following settings: MS1: 400-1500 Th, 70,000 resolution, $1x10^6$ AGC target, 250 ms maximum

injection time. MS2: HCD fragmentation (NCE 30) with fragment ions scanning from m/z 200, $8x10^3$AGC target. Dynamic exclusion was set to ± 10 ppm for 30 s. To identify possible modifications of RICTOR, raw files were processed using PEAKS Studio (version 8.0, Bioinformatics Solutions Inc.) with the following parameters: Trypsin digestion; Human database (UniProt reference proteome downloaded 18 Dec 2018 containing 21066 proteins) with additional contaminant database (containing 246 common contaminants); oxidation (M) and carbamidomethylation (C) as variable modifications at the PEAKS DB stage, 483 PEAKS built-in modifications at the PEAKS PTM stage; amino acid mutations identification enabled at the SPIDER stage.

QUANTIFICATION AND STATISTICAL ANALYSIS

Significance levels for comparisons between groups with paired or unpaired two- or one-tailed Student's t test or one-way ANOVA with Tukey post hoc test was performed using Microsoft Excel and GraphPad Prism v7. Information on number of replicates (n) and p values are provided in the figure legends. Error bars shown in the figures represent a standard error of the mean (SEM). Sample sizes were chosen on the basis of extensive experience with the assay performed.